13. Wysession, M. E., *et al.* in *The Core-Mantle Boundary Region* (eds Gurnis, M., Wysession, M. E., Knittle, E. & Buffett, B. A.) 273–297 (American Geophysical Union, Washington DC, 1998).
14. Sidorin, I., Gurnis, M. & Helmberger, D. V. Evidence for a ubiquitous seismic discontinuity at the base of the mantle. *Science* **286,** 1326–1331 (1999).
15. Lay, T., Williams, Q., Garnero, E. J., Kellogg, L. & Wysession, M. E. in *The Core-Mantle Boundary Region* (eds Gurnis, M., Wysession, M. E., Knittle, E. & Buffett, B. A.) 299–318 (American Geophysical Union, Washington DC, 1998).
16. Panning, M. & Romanowicz, B. Inferences on flow at the base of Earth's mantle based on seismic anisotropy. *Science* **303,** 351–353 (2004).
17. Montagner, J. P. & Nataf, H. C. A simple method for inverting the azimuthal anisotropy of surface waves. *J. Geophys. Res.* **91,** 511–520 (1986).
18. Wentzcovitch, R. M., Karki, B. B., Karato, S. & Da Silva, C. R. S. High pressure elastic anisotropy of $MgSiO_3$ perovskite and geophysical implications. *Earth Planet. Sci. Lett.* **164,** 371–378 (1998).
19. Karato, S., Zhang, S. & Wenk, H. R. Superplasticity in Earth's lower mantle: evidence from seismic anisotropy and rock physics. *Science* **270,** 458–461 (1995).
20. Masters, G. & Laske, G. in *Earth's Deep Interior: Mineral Physics and Tomography from the Atomic to the Global Scale* (eds Karato, S., Forte, A., Liebermann, R., Masters, G. & Stixrude, L.) 63–87 (American Geophysical Union, Washington DC, 2000).
21. Oganov, A. R., Brodholt, J. P. & Price, G. D. The elastic constants of $MgSiO_3$ perovskite at pressures and temperatures of the Earth's mantle. *Nature* **411,** 934–937 (2001).
22. Wentzcovitch, R. M., Karki, B. B., Cococcioni, M. & de Gironcoli, S. Thermoelastic properties of $MgSiO_3$-perovskite: insights on the nature of the Earth's lower mantle. *Phys. Rev. Lett.* **92,** 018501 (2004).
23. Murakami, M. *Phase Transition of Lower Mantle Mineral and its Geophysical Implications* Thesis, Tokyo Institute of Technology (2004).
24. Vanderbilt, D. Soft self-consistent pseudopotentials in a generalized eigenvalue formalism. *Phys. Rev. B* **41,** 7892–7895 (1990).
25. Civalleri, B. & Harrison, N. M. New ultrasoft pseudopotentials for the study of silicates. *Mol. Simulat.* **28,** 213–237 (2002).
26. Brodholt, J. P., Organov, A. R. & Price, G. D. Computational mineral physics and the physical properties of perovskite. *Phil. Trans. R. Soc. Lond. A* **360,** 2507–2520 (2002).
27. Monkhorst, H. J. & Pack, J. D. Special points for Brillouin-zone integrations. *Phys. Rev. B* **13,** 5188–5192 (1976).
28. Nielsen, O. H. & Martin, R. M. First principles calculation of stress. *Phys. Rev. Lett.* **50,** 697–700 (1983).
29. Francis, G. P. & Payne, M. C. Finite basis set corrections to total energy pseudopotential calculations. *J. Phys. Condens. Matter* **2,** 4395–4404 (1990).
30. Iitaka, T. & Ebisuzaki, T. First-principles calculation of elastic properties of solid argon at high pressures. *Phys. Rev. B* **65,** 012103 (2002).

Supplementary Information accompanies the paper on **www.nature.com/nature**.

Acknowledgements We thank S. Kaneshima for discussions, D.M. Bird for providing CASTEP codes, N.M. Harrison for pseudopotentials and the computer centres of RIKEN and NIG for access to the supercomputers. This work was also supported by JASRI/SPring-8 and IFREE/JAMSTEC.

Competing interests statement The authors declare that they have no competing financial interests.

Correspondence and requests for materials should be addressed to T.I. (tiitaka@riken.jp).

Theoretical and experimental evidence for a post-perovskite phase of $MgSiO_3$ in Earth's D″ layer

Artem R. Oganov[1] **& Shigeaki Ono**[2]

[1]*Laboratory of Crystallography, Department of Materials, ETH Zurich, Wolfgang Pauli Strasse 10, CH-8093 Zurich, Switzerland*
[2]*Institute for Frontier Research on Earth Evolution, Japan Agency for Marine-Earth Science and Technology, 2-15 Natsushima-cho, Yokosuka-shi, Kanagawa 237-0061, Japan*

The Earth's lower mantle is believed to be composed mainly of $(Mg,Fe)SiO_3$ perovskite, with lesser amounts of (Mg,Fe)O and $CaSiO_3$ (ref. 1). But it has not been possible to explain many unusual properties of the lowermost ~150 km of the mantle (the D″ layer) with this mineralogy. Here, using *ab initio* simulations and high-pressure experiments, we show that at pressures and temperatures of the D″ layer, $MgSiO_3$ transforms from perovskite into a layered $CaIrO_3$-type post-perovskite phase. The elastic properties of the post-perovskite phase and its stability field explain several observed puzzling properties of the D″ layer: its seismic anisotropy[2], the strongly undulating shear-wave discontinuity at its top[3–6] and possibly the anticorrelation between shear and bulk sound velocities[7,8].

If $MgSiO_3$ perovskite is stable throughout the lower mantle, it should be the most abundant mineral in our planet. While some researchers[9] have suggested its decomposition into the oxides at lower mantle conditions, most workers[10–13] have found that perovskite is more stable than the oxides. To our knowledge, the possibility that $MgSiO_3$ could be stable in a completely new structure within the lower mantle has not been considered.

The shear-wave discontinuity at the top of the D″ layer, suggested in ref. 3, has a strong topography. This discontinuity has commonly been explained by some chemical difference between the D″ layer and the rest of the lower mantle. However, using a combination of dynamical and seismic modelling, Sidorin *et al.*[4–6] have shown that the most consistent explanation is a phase transition in mantle minerals. Their best model[5,6] had a shear-wave discontinuity of ~1% located ~150 km above the core–mantle boundary (depth 2,740 km), with a Clapeyron slope of $6\,MPa\,K^{-1}$ (though values as large as $10\,MPa\,K^{-1}$ were almost equally acceptable). The discontinuities of the compressional wave velocities and of the density could not be resolved. The models of Sidorin *et al.*[4–6] were very appealing, but the major problem was that no appropriate phase transition was known at the time. Here we show that $MgSiO_3$ perovskite undergoes a structural phase transition at the conditions corresponding to the top of the D″ layer. The predicted seismic signatures of this transition match the seismological inferences of Sidorin *et al.*[4–6].

A key observation made by Ono *et al.*[14] was that Fe_2O_3, like $MgSiO_3$, transforms from the corundum (or ilmenite) to the perovskite structure under pressure. As these authors further found[14], a post-perovskite phase of Fe_2O_3 with a $CaIrO_3$-type *Cmcm* structure[15] (Fig. 1) is stable above 60 GPa. This has led to the idea that a similar structure could be stable for $MgSiO_3$ at high pressure.

We explored this idea using *ab initio* simulations based on density functional theory within the local density approximation

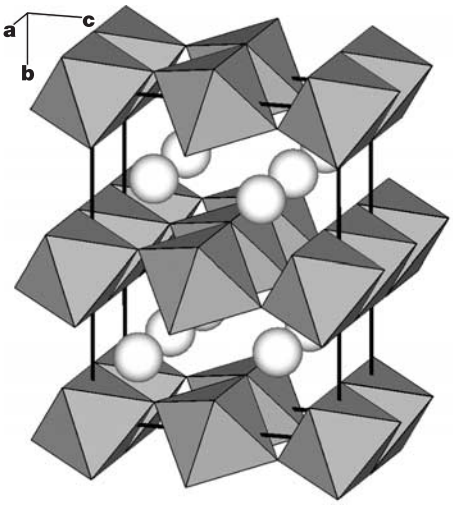

Figure 1 Structure of the post-perovskite phase of $MgSiO_3$ (calculated at 120 GPa). SiO_6 octahedra and Mg atoms (spheres) are shown. Similar structures are known for Fe_2O_3, $CaIrO_3$, $FeUS_3$, $PbTlI_3$, $USeS_3$, $KTmI_3$, $AgTaS_3$ and $CaInBr_3$.

(LDA) and the generalized gradient approximation[16] (GGA). The calculated enthalpy difference (Fig. 2a) indicates that for pure $MgSiO_3$ the $CaIrO_3$-structured phase becomes thermodynamically more stable than perovskite well within the range of lower-mantle pressures: at 83.7 GPa in the LDA or at 98.7 GPa in the GGA. It is well known[17] that usually the LDA underestimates transition pressures, whereas the GGA slightly (by a few GPa) overestimates them.

The Clapeyron slope was calculated using density-functional perturbation theory[18] to be 9.85 MPa K^{-1} within the LDA and 9.56 MPa K^{-1} within the GGA. These numbers agree with a simple formula for the high-temperature entropy change[19] for transitions without coordination number changes (as in this case): $\Delta S = 3nk_B\gamma(\Delta V/V)$, where n is the number of atoms in volume V, ΔV the volume change at transition, k_B the Boltzmann constant, and γ the Grüneisen parameter at the transition (1.2 for perovskite[20,21]). This formula yields a Clapeyron slope of ~8 MPa K^{-1}.

Following this prediction, we found the new phase experimentally. A sample of pure $MgSiO_3$ was heated with a laser to overcome potential kinetic effects on possible phase transitions. Experimental details have been described elsewhere[13,22]. The experimental powder diffraction pattern is shown in Fig. 3; we could index reflections not belonging to platinum, platinum carbide, and rhenium gasket in the *Cmcm* space group with lattice parameters very similar to the theoretical ones (Table 1). This confirms the predicted stability of the post-perovskite phase in pure $MgSiO_3$. Note that the calculated and experimentally determined stability fields are in excellent agreement with each other (Fig. 2b). At temperatures of the D″ layer (~3,000 K) the GGA transition pressure is 127 GPa, which corresponds to the top of the D″ layer, 2,740 km depth. We recall that Sidorin *et al.*[4–6] suggested a transition at 127 GPa with a Clapeyron slope of 6 MPa K^{-1}.

Equation of state parameters for perovskite and post-perovskite are listed in Table 2, and the elastic constants calculated from stress–

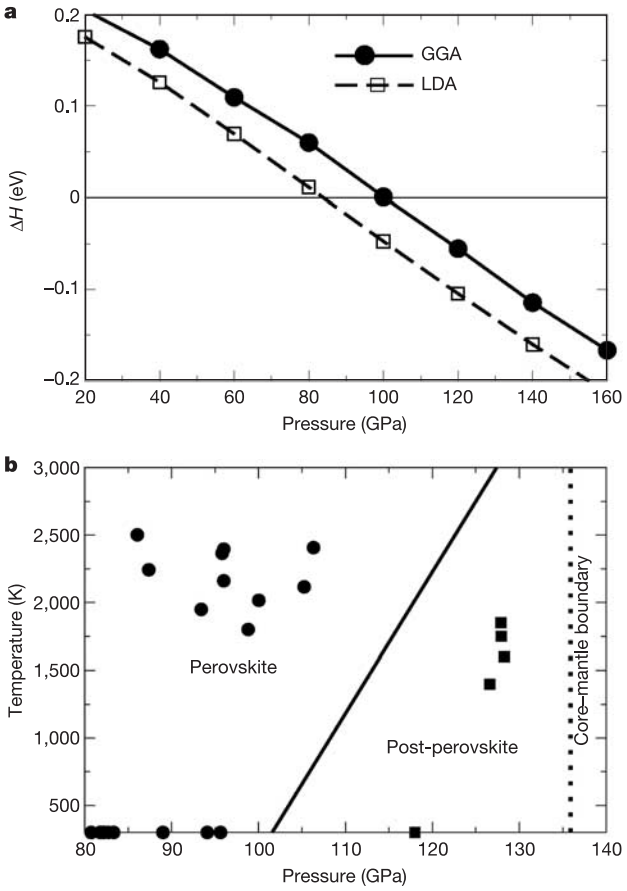

Figure 2 Stability of the post-perovskite phase. **a**, Static enthalpy difference showing a phase transition at 98.7(83.7) GPa in the GGA(LDA). GGA calculations used the all-electron PAW method[27,28] as implemented in the VASP code[29], with $1s^2 2s^2$ core (radius 2 a.u.) for Mg, $1s^2 2s^2 2p^6$ core (radius 1.5 a.u.) for Si, $1s^2$ core (radius 1.52 a.u.) for O. With a plane wave cut-off of 500 eV and the Brillouin zone sampled by Monkhorst-Pack grids, 4 × 4 × 4 for perovskite and 6 × 6 × 4 for post-perovskite (for the latter we used the primitive cell with 10 atoms), total energy differences and pressure are converged to 0.006 meV per atom and 0.25 GPa, respectively. Structural relaxation was done using conjugate gradients, until the total energy changes were below 10^{-4} eV. The fully converged LDA calculations were done using the ABINIT code[30] (ABINIT is a common project of the Université Catholique de Louvain, Corning Inc. and other contributors; http://www.abinit.org). These calculations used Troullier-Martins pseudopotentials, plane waves with a cut-off of 1,088 eV, and the same Monkhorst-Pack grids as in the GGA case. **b**, Pressure–temperature phase diagram: theory and experiment. Experimental points: perovskite (ref. 13) for mantle composition (KLB-1 peridotite), post-perovskite for pure $MgSiO_3$. The solid line is based on the static transition pressure (98.7 GPa) and a Clapeyron slope of 9.56 MPa K^{-1} calculated using density-functional perturbation theory and the GGA, with the ABINIT code[30]. In these calculations, the dynamical matrices were calculated on 2 × 2 × 2 and 3 × 3 × 2 grids in the Brillouin zone for perovskite and post-perovskite, respectively, using density-functional perturbation theory[18]. Interpolating these throughout the Brillouin zone, we calculated phonon frequencies at a very dense reciprocal-space mesh. Errors in the calculated frequencies are within 5 cm^{-1} (mostly less than 1 cm^{-1}). From the resulting phonon spectra we calculated various thermodynamic properties, including the entropy (S) of each phase and the high-temperature Clapeyron slope $dP/dT = \Delta S/\Delta V$.

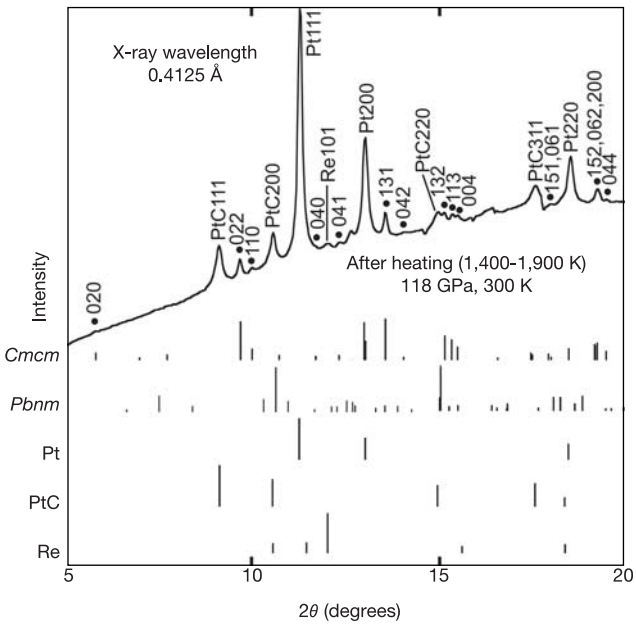

Figure 3 Experimental powder diffraction pattern at 118 GPa and 300 K matching the predicted lattice parameters. The sample was heated with a TEM01-mode YLF laser from two sides without a pressure transmitting medium. The pressure was determined using the reference equation of state of platinum (which was mixed with the sample). The sample temperatures were measured from two sides using the spectroradiometric method. The samples were probed using an angle-dispersive X-ray diffraction technique at the synchrotron beam line BL10XU, SPring-8 in Japan. Filled circles, post-perovskite; Pt, platinum used as an internal pressure calibrant; Re, rhenium of the gasket; PtC, platinum carbide. Observed unit cell dimensions of post-perovskite are $a = 2.471(4)$ Å, $b = 8.091(12)$ Å, $c = 6.110(11)$ Å, $V = 122.16(34)$ Å^3. Observed volume change from perovskite to post-perovskite is 0.9%. Vertical bars indicate the calculated positions of the diffraction lines of *Cmcm* post-perovskite phase, *Pbnm* perovskite, platinum, NaCl-type platinum carbide, and rhenium gasket.

strain relations at 120 GPa are given in Table 3. The density discontinuity at the transition is 1.4%; for the mantle the expected density discontinuity is 1.1%. The predicted shear wave discontinuity in $MgSiO_3$ is 1.9% (1.4% for the mantle), consistent with ~1% suggested by Sidorin *et al.*[4–6]. We predict a very small discontinuity for the compressional wave velocity (0.3% for pure $MgSiO_3$), explaining why it was so seldom found at the top of the D″ layer[4–6].

The calculated properties of our new phase explain many puzzling features of the D″ layer. In seismological models, horizontally polarized shear waves are faster (by 1% on average[2]) than the vertically polarized ones ($v_{SH} > v_{SV}$). Significant seismic anisotropy of the D″ layer, containing a signature of the convective flow[2], could not be explained even qualitatively by mineral physics[23,24]. The structure of the post-perovskite phase has silicate layers parallel to {010}, which is then the most natural slip plane that will be oriented parallel to the convective flow. In regions of horizontal flow (most of D″), we obtain $v_{SH}/v_{SV} = 1.029 > 1$ for post-perovskite (using the method of ref. 25 and data of Table 3). This is consistent with seismological evidence, and suggests either a large degree of lattice-preferred orientation or significant contributions from other sources such as shape-preferred orientation (anisotropy due to the ordered distribution of crystals and inclusions in the rock). In regions of upwelling convective streams (for example, below the central Pacific), slip planes would be predominantly vertical and one would obtain $v_{SH} < v_{SV}$, actually observed in such regions[2].

Another mystery of D″, the anticorrelation between the shear (v_S) and bulk sound (v_ϕ) velocities[7,8], can also be quantitatively explained by the phase transition of $MgSiO_3$ from perovskite into the post-perovskite phase. We recall that it has been difficult to explain why, at a given depth in the lowermost mantle, anomalies of v_S and v_ϕ have opposite signs. As Table 3 shows, the post-perovskite transition has a positive jump of v_S and a negative jump of v_ϕ. Note that the transition is first order, and in a multicomponent system such as the Earth' mantle there will be an interval ΔT of coexistence of the two phases at given pressure. For this two-phase region, we can write:

$$\left(\frac{\partial v_\phi}{\partial v_S}\right)_P \approx \frac{\left(\frac{\partial v_\phi}{\partial T}\right)_{P,x} + f\frac{v_{\phi 2} - v_{\phi 1}}{\Delta T}}{\left(\frac{\partial v_S}{\partial T}\right)_{P,x} + f\frac{v_{S2} - v_{S1}}{\Delta T}} \quad (1)$$

which includes purely thermal responses (at given composition x and pressure P) of the velocities and effects due to a phase transition; f is the volume fraction of $MgSiO_3$ (75%). The poorly known effects of variation of Al and Fe content are not included in equation (1), but we find that anticorrelation can be explained without them. Using equation (1), data of Table 3, and assuming thermal responses equal to those of perovskite[20], we get $(\partial \ln v_S/\partial \ln v_\phi)_P = -0.15$ and -0.33 for $\Delta T = 250$ K and 50 K, respectively (from seismic tomography: -0.15 (ref. 8) and -0.3 (ref. 7)). Furthermore, we can reproduce the positive correlation between the shear and compressional (v_P) velocities with the same ΔT: $(\partial \ln v_S/\partial \ln v_P)_P = 3.36$ for $\Delta T = 250$ K (3.3 from ref. 8).

The fact that so many previously unexplained seismic features of the D″ layer (seismic discontinuity, its magnitude and Clapeyron slope, anisotropy, bulk-shear velocity anticorrelation) are naturally explained by the properties of post-perovskite is a strong indication that this phase is indeed the major component of the D″ layer. The D″ layer is not necessarily chemically very different from the rest of the lower mantle, but it surely is different mineralogically. Neither theoretical and experimental error bars (a few GPa for transition pressure) nor the effects of temperature as explored here would change our prediction that the $CaIrO_3$-type post-perovskite phase is stable in the D″ layer. At present, very little is known about the effects of Fe^{2+}, Fe^{3+} and Al^{3+} impurities on mantle minerals. We expect that at least Fe^{3+} impurities should stabilize the post-perovskite phase against perovskite; this is because at high pressure Fe_2O_3 also has the $CaIrO_3$ structure[14].

Our findings have other implications. For instance, rheological properties of post-perovskite (probably very different from those of perovskite) and the predicted density discontinuity (1.1%) at top of the D″ layer could be important for mantle dynamics. Also, element partitioning between post-perovskite, perovskite, and molten Fe might be a key to some geochemical anomalies. Elements that are incompatible in the mantle (for example, Na, K, U, Th) might be more easily accommodated in the layered post-perovskite structure, which may affect the chemistry of plume magmas. As Fe_2O_3 at high pressure has the same structure as post-perovskite, post-perovskite could have a greater concentration of Fe^{3+} than perovskite. It is also likely that the size of the D″ region increased significantly with time as the mantle cooled down; this is because the Clapeyron slope of the post-perovskite transition is large, 8.0–9.6 MPa K^{-1}. If the whole mantle had been molten with temperatures above 4,000–4,500 K in the early history of the Earth, it would be perovskite that crystallized from the cooling melt, and only on further cooling would post-perovskite and the D″ layer have appeared. The present-day thickness of the D″ could be used to estimate its age, given the cooling history of the lowermost mantle. As post-perovskite stability requires pressures unattainable in smaller planets like Mercury

Table 1 **Structures of post-perovskite and perovskite at 120 GPa**

	Post-perovskite*				Perovskite†		
Mg	0	0.2532	1/4	**Mg**	0.5246	0.5768	1/4
Si	0	0	0	**Si**	1/4	0	1/4
O1	0	0.9276	1/4	**O1**	0.1164	0.4669	1/4
O2	0	0.6356	0.4413	**O2**	0.1829	0.1926	0.5575

Table shows GGA results.
*Space group *Cmcm*: $a = 2.474$ Å, $b = 8.121$ Å, $c = 6.138$ Å; distances (in Å): Mg–O1 = 1.880 (×2), Mg–O2 = 1.955(×4), 2.099(×2); Si–O1 = 1.643 (×2), Si–O2 = 1.695 (×4).
†Space group *Pbnm*: $a = 4.318$ Å, $b = 4.595$ Å, $c = 6.305$ Å; distances (in Å): Mg–O1 = 1.833(×1), 1.893(×1), Mg–O2 = 1.864(×2), 2.047(×2), 2.201(×2); Si–O1 = 1.661(×2), Si–O2 = 1.659(×2), 1.670(×2).

Table 2 **Vinet equations of state of perovskite and post-perovskite**

Parameters	Post-perovskite		Perovskite		Exp.*
	LDA	GGA	LDA	GGA	
V_0 (Å^3)	162.86	167.64	163.35	167.42	162.3
K_0 (GPa)	231.93	199.96	259.82	230.05	259.5
K_0'	4.430	4.541	4.060	4.142	3.69

*Third-order Birch-Murnaghan equation of state parameters at room temperature[10].

Table 3 **Elastic constants of perovskite and post-perovskite at 120 GPa**

	C_{11}	C_{22}	C_{33}	C_{12}	C_{13}	C_{23}	C_{44}	C_{55}	C_{66}	K	G
Perovskite*	907	1,157	1,104	513	406	431	364	271	333	648.0	310.9
Post-perovskite†	1,252	929	1,233	414	325	478	277	266	408	647.2	327.5

Table shows GGA results. All elastic constants are in GPa.
*Acoustic velocities (m s^{-1}): $v_P = 14{,}118$; $v_S = 7{,}636$; $v_\phi = 11{,}026$.
†Acoustic velocities (m s^{-1}): $v_P = 14{,}158$; $v_S = 7{,}783$, $v_\phi = 10{,}940$.

and Mars, many features of these planets would be different from those of the Earth. Further studies are necessary to address these and other issues (elasticity and anelasticity, electrical conductivity, radiative conductivity, energetics of stacking faults, effects of impurities on stability and properties of post-perovskite). Finally, we note that the results of a recent, independent, experimental study[26] of the post-perovskite phase transition are consistent with our theoretical and experimental findings. □

Received 24 March; accepted 27 May 2004; doi:10.1038/nature02701.

1. Fiquet, G. Mineral phases of the Earth's mantle. *Z. Krist.* **216,** 248–271 (2001).
2. Panning, M. & Romanowicz, B. Inferences on flow at the base of Earth's mantle based on seismic anisotropy. *Science* **303,** 351–353 (2004).
3. Lay, T. & Helmberger, D. V. A shear velocity discontinuity in the lower mantle. *Geophys. Res. Lett.* **10,** 63–66 (1983).
4. Sidorin, I., Gurnis, M., Helmberger, D. V. & Ding, X. Interpreting $D^{\prime\prime}$ seismic structure using synthetic waveforms computed from dynamic models. *Earth Planet. Sci. Lett.* **163,** 31–41 (1998).
5. Sidorin, I., Gurnis, M. & Helmberger, D. V. Evidence for a ubiquitous seismic discontinuity at the base of the mantle. *Science* **286,** 1326–1331 (1999).
6. Sidorin, I., Gurnis, M. & Helmberger, D. V. Dynamics of a phase change at the base of the mantle consistent with seismological observations. *J. Geophys. Res.* **104,** 15005–15023 (1999).
7. Su, W. J. & Dziewonski, A. M. Simultaneous inversion for 3-D variations in shear and bulk velocity in the mantle. *Phys. Earth Planet. Inter.* **100,** 135–156 (1997).
8. Masters, G. *et al.* in *Earth's Deep Interior: Mineral Physics and Tomography from the Atomic to the Global Scale* (ed. Karato, S.-i.) 63–87 (AGU Geophysical Monograph 117, American Geophysical Union, Washington DC, 2000).
9. Saxena, S. K. *et al.* Stability of perovskite ($MgSiO_3$) in the Earth's mantle. *Science* **274,** 1357–1359 (1996).
10. Fiquet, G., Dewaele, A., Andrault, D., Kunz, M. & Le Bihan, T. Thermoelastic properties and crystal structure of $MgSiO_3$ perovskite at lower mantle pressure and temperature conditions. *Geophys. Res. Lett.* **27,** 21–24 (2000).
11. Serghiou, G., Zerr, A. & Boehler, R. $(Mg,Fe)SiO_3$-perovskite stability under lower mantle conditions. *Science* **280,** 2093–2095 (1998).
12. Shim, S. H., Duffy, T. S. & Shen, G. Y. Stability and structure of $MgSiO_3$ perovskite to 2300-kilometer depth in Earth's mantle. *Science* **293,** 2437–2440 (2001).
13. Ono, S., Ohishi, Y. & Mibe, K. Phase transition of Ca-perovskite and stability of Al-bearing Mg-perovskite in the lower mantle. *Am. Mineral.* (in the press).
14. Ono, S., Sata, N. & Ohishi, Y. Phase transformation of perovskite structure in Fe_2O_3 at high pressures and high temperatures. *Am. Mineral.* (submitted).
15. Rodi, F. & Babel, D. Erdalkaliiridium(IV) - oxide: Kristallstruktur von $CaIrO_3$. *Z. Anorg. Allg. Chem.* **336,** 17–23 (1965).
16. Perdew, J. P., Burke, K. & Ernzerhof, M. Generalized gradient approximation made simple. *Phys. Rev. Lett.* **77,** 3865–3868 (1996).
17. Oganov, A. R. & Brodholt, J. P. High-pressure phases in the Al_2SiO_5 system and the problem of Al-phase in Earth's lower mantle: ab initio pseudopotential calculations. *Phys. Chem. Miner.* **27,** 430–439 (2000).
18. Baroni, S., de Gironcoli, S., Dal Corso, A. & Gianozzi, P. Phonons and related crystal properties from density-functional perturbation theory. *Rev. Mod. Phys.* **73,** 515–562 (2001).
19. Urusov, V. S. *Theoretical Crystal Chemistry* (Moscow State Univ. Press, Moscow, 1987) [in Russian].
20. Oganov, A. R., Brodholt, J. P. & Price, G. D. The elastic constants of $MgSiO_3$ perovskite at pressures and temperatures of the Earth's mantle. *Nature* **411,** 934–937 (2001).
21. Oganov, A. R., Brodholt, J. P. & Price, G. D. Ab initio elasticity and thermal equation of state of $MgSiO_3$ perovskite. *Earth Planet. Sci. Lett.* **184,** 555–560 (2001).
22. Ono, S., Hirose, K., Isshiki, M., Mibe, K. & Saito, Y. Equation of state of hexagonal aluminous phase of natural composition to 63 GPa at 300 K. *Phys. Chem. Miner.* **29,** 527–531 (2002).
23. Jeanloz, R. & Williams, Q. The core-mantle boundary region. *Rev. Mineral.* **37,** 241–259 (1998).
24. Wentzcovitch, R. M., Karki, B. B., Karato, S. & da Silva, C. R. S. High pressure elastic anisotropy of $MgSiO_3$ perovskite and geophysical implications. *Earth Planet. Sci. Lett.* **164,** 371–378 (1998).
25. Montagner, J.-P. & Nataf, H.-C. A simple method for inverting the azimuthal anisotropy of surface waves. *J. Geophys. Res.* **91,** 511–520 (1986).
26. Murakami, M., Hirose, K., Kawamura, K., Sata, N. & Ohishi, Y. Post-perovskite phase transition in $MgSiO_3$. *Science* **304,** 855–858 (2004).
27. Blöchl, P. E. Projector augmented-wave method. *Phys. Rev. B* **50,** 17953–17979 (1994).
28. Kresse, G. & Joubert, D. From ultrasoft pseudopotentials to the projector augmented-wave method. *Phys. Rev. B* **59,** 1758–1775 (1999).
29. Kresse, G. & Furthmüller, J. Efficiency of ab initio total-energy calculations for metals and semiconductors using a plane-wave basis set. *Comp. Mater. Sci.* **6,** 15–50 (1996).
30. Gonze, X. *et al.* First-principles computation of materials properties: the ABINIT software project. *Comp. Mater. Sci.* **25,** 478–492 (2002).

Acknowledgements Calculations were performed at CSCS (Manno) and ETH Zurich. We thank P. Ulmer, A.N. Halliday, S. Goes, F. Cammarano, A.B. Thompson and P.J. Tackley for discussions, and Y. Ohishi and N. Sata for experimental support. Synchrotron radiation experiments were performed at the BL10XU, SPring-8.

Competing interests statement The authors declare that they have no competing financial interests.

Correspondence and requests for materials should be addressed to A.R.O. (a.oganov@mat.ethz.ch).

Audience drives male songbird response to partner's voice

Clémentine Vignal[1,2], Nicolas Mathevon[1] & Stéphane Mottin[2]

[1]*Equipe 'Communications Acoustiques' NAMC CNRS UMR8620, Université Paris XI-Orsay and LBA Université Jean Monnet, 42023 Saint-Etienne Cedex 2, France*
[2]*TSI CNRS UMR5516 Université Jean Monnet, 42023 Saint-Etienne Cedex 2, France*

According to the social intelligence hypothesis, social context represents an important force driving the selection of animal cognitive abilities such as the capacity to estimate the nature of the social relationships between other individuals[1–4]. Despite this importance, the influence of this force has been assessed only in primates and never in other animals showing social interactions[5–7]. In this way, avian communication generally takes place in a network of signallers and receivers, which represents an audience altering individual signalling behaviours[8,9]. Indeed, vocal amplitude[10] and repertoire[11] are known to be socially regulated and the attitude towards the opposite sex may change depending on the audience[8,12,13]. This 'audience effect'[8,14–16] provides support for the reality of social awareness in some bird species. However no evidence has yet been found to suggest that birds are able to estimate the characteristics of the social relationships between group-mates. Here we show that the male of a gregarious songbird species—the zebra finch (*Taeniopygia guttata*)—pays attention to the mating status of conspecific pairs, and uses this information to control its behaviour towards its female partner.

Zebra finches are monogamous flock-forming birds that seem to use acoustic recognition for pair-bond maintenance[11,17]. A number of different vocalizations are produced by this species[11], distance calls being the most frequently emitted by both males and females. Distance calls are used by the members of a pair to remain in contact when the flock is foraging or feeding and especially when the birds lose visual contact with each other[11]. As in many gregarious species, vocal recognition is thus likely to be a key component of reproductive success and it should be supported in both sexes by acoustic cues of distance calls[18–20]. Previous laboratory experiments testing isolated birds demonstrated that the female zebra finch is able to recognize its mate's vocalizations from other males' vocalizations[17], but never succeeded in demonstrating a mutual acoustic recognition between mates[11]. In the natural biological context described above, it is very unlikely that wild male zebra finches do not recognize their mates' voices. Two main hypotheses can thus be envisaged: either captive zebra finches have lost some cognitive capacities because of domestication (for instance, females' calls may be less individualized, and/or males may no longer be able to recognize them), or tested males do not show preferential response to their mate's voice owing to a modification of their natural behaviour by their socially isolated position during the playback tests. Indeed social isolation could be a situation of stress in comparison to the natural context where the zebra finch lives in large groups and experiences permanent social interactions that may influence mate-directed behaviour.

To determine whether the vocalizations of female zebra finches support mate recognition, we analysed the acoustic structure of distance calls, searching for acoustic cues which could encode the emitter's individual identity. The female distance call is a complex sound with a fundamental frequency associated with several harmonics (Fig. 1a). This sound is frequency- and amplitude-modulated. With reference to frequency-modulation characteristics, the distance call can be divided into three segments of